
Article:
Schiantella, M., Gilbert, M., Smith, C.C. et al. (2024) Limit analysis of 2D non-periodic masonry walls via discontinuity layout optimization. International Journal of Architectural Heritage, 19 (10). pp. 2422-2442. ISSN: 1558-3058

https://doi.org/10.1080/15583058.2024.2437633

International Journal of Architectural Heritage
Conservation, Analysis, and Restoration

ISSN: (Print) (Online) Journal homepage: www.tandfonline.com/journals/uarc20

Limit Analysis of 2D Non-Periodic Masonry Walls via Discontinuity Layout Optimization

Mattia Schiantella, Matthew Gilbert, Colin C. Smith, Linwei He & Federico Cluni

To cite this article: Mattia Schiantella, Matthew Gilbert, Colin C. Smith, Linwei He & Federico Cluni (20 Dec 2024): Limit Analysis of 2D Non-Periodic Masonry Walls via Discontinuity Layout Optimization, International Journal of Architectural Heritage, DOI: 10.1080/15583058.2024.2437633

To link to this article: https://doi.org/10.1080/15583058.2024.2437633

Published online: 20 Dec 2024.

INTERNATIONAL JOURNAL OF ARCHITECTURAL HERITAGE
https://doi.org/10.1080/15583058.2024.2437633

Taylor & Francis
Taylor & Francis Group

RESEARCH ARTICLE

OPEN ACCESS Check for updates

Limit Analysis of 2D Non-Periodic Masonry Walls via Discontinuity Layout Optimization

Mattia Schiantella [a], Matthew Gilbert [b], Colin C. Smith [b], Linwei He [b], and Federico Cluni [a]

[a]Department of Civil and Environmental Engineering, University of Perugia, Perugia, Italy; [b]School of Mechanical, Aerospace and Civil Engineering, University of Sheffield, Sheffield, UK

ABSTRACT

Many historic masonry constructions comprise elements formed using brick or stone masonry units arranged in an irregular, or *non-periodic* bonding pattern. However, when the arrangement of units is not completely random the texture is frequently referred to as *quasi-periodic*; such masonry is a key focus in this work. However, the influence of any non-periodicity on structural performance can be difficult to establish. In this contribution, the discontinuity layout optimization (DLO) numerical limit analysis procedure is used to investigate the influence of non-periodicity on structural performance. Both discrete and smeared continuum representations of the masonry are considered and applied to a range of representative example problems, including in-plane analysis of square panels and more complex buildings under horizontal seismic action and rigid settlement. Although the discrete, rigid block method can be used to compare the performance of different textures, it requires the whole wall to be modelled in detail; this is not required with the proposed DLO smeared continuum representation. Various example problems are considered, indicating that the smeared continuum representation allows conservative solutions to be obtained for problems involving quasi-periodic masonry

ARTICLE HISTORY
Received 7 August 2024
Accepted 25 November 2024

KEYWORDS
In-plane behaviour; limit analysis; Masonry; non-periodic

1. Introduction

The walls of historical masonry buildings were often constructed using irregular bonding patterns. Although the interior of such walls may comprise rubble or even earth elements (Binda et al. 2006), these tend to disaggregate under seismic actions and are therefore typically ignored for the purposes of analysis. These buildings were generally designed to carry gravity loads, without concern for seismic actions. Moreover, over the centuries historical buildings have often been subject to modifications that have altered the distribution of loads, and potentially the effectiveness of the structure. It is therefore important that the analysis models applied to such structures reflect this (D'Ayala and Speranza 2003).

When analysing a historic masonry construction, a suitable model for the constituent masonry material must be chosen. This is often not straightforward, particularly if the masonry comprises units (e.g. bricks or stone blocks) that are not arranged in a regular periodic pattern. Sometimes the bonding pattern will be quasi-periodic, that is to say, courses of a given height are present, though the units within a course may have different lengths, and the heights of different courses may also vary. Alternatively, the bonding pattern may be completely erratic with no discernible bedding courses evident.

Masonry structures are commonly modelled using either discrete or smeared continuum representations. In the former case, masonry units are modelled explicitly, enabling non-periodic bonding patterns to be represented directly. Mortar joints are also modelled explicitly, though for the sake of simplicity, they may be assumed to have zero thickness — used in conjunction with geometrically expanded units. Examples in the framework of limit analysis include the methods proposed by Livesley (1978), Ferris and Tin-Loi (2001), and Gilbert, Casapulla, and Ahmed (2006), where in the latter two contributions, non-associative friction was considered. Discrete modelling has also been widely investigated beyond the domain of limit analysis, e.g. by applying the discrete element method (DEM) (Cundall and Strack 1979). Contributions for masonry constructions can be found in Lemos (2007), with validation data presented in Bui et al. (2017).However, since a typical masonry structure consists of many thousands of masonry units, it can be computationally expensive to model all units individually with discrete modelling approaches. Thus, alternative smeared continuum formulations have also been developed. Considering periodic masonry, early contributions include

CONTACT Linwei He linwei.he@sheffield.ac.uk School of Mechanical, Aerospace and Civil Engineering, University of Sheffield, Sheffield, S1 3JD, UK

those of Pande, Liang, and Middleton (1989) and Anthoine (1995). A key development was the use of a unit cell or representative volume element (RVE) to ensure that specific masonry properties are properly represented. Considering non-periodic masonry, Cluni and Gusella (2004) used RVEs in conjunction with 'test-windows' of increasing dimensions to capture the elastic properties of the masonry. This was later extended by Cavalagli, Cluni, and Gusella (2011) to enable the strength of the masonry element to be determined.

Considering quasi-periodic masonry, the concept of a statistically equivalent periodic unit cell (SEPUC) was proposed by Sejnoha et al. (2008). For the analysis of non-periodic masonry walls subjected to in-plane loading, Tiberti and Milani (2019) proposed a workflow that starts with a digital image of a wall. A limit analysis procedure is then performed, employing automatically generated homogenized yield surfaces based on the pixel distribution. This approach has now also been extended to treat out-of-plane loading scenarios (Tiberti and Milani 2020). Moreover, Funari et al. (2022) proposed a new analytical model for macro-block limit analysis of in-plane failure mechanisms in non-periodic masonry structures. This model utilises measurable masonry quality indexes to compute frictional resistance and predict collapse.

In this paper, the discontinuity layout optimization (DLO) numerical limit analysis is employed to compare the in-plane load-carrying capacities of periodic and non-periodic masonry elements (as in Schiantella, Cluni, and Gusella 2022). DLO is a highly efficient method for identifying the critical layout of sliding/opening discontinuities that form a mechanism at failure of a solid or structure, utilising the well-established layout optimization technique. Unlike finite element limit analysis (Milani, Lourenço, and Tralli 2006), with DLO (Smith and Gilbert 2007), singularities in the stress or displacement fields can be handled in a direct and natural manner, obviating the need for tailored meshes or adaptive mesh refinement (e.g. Lyamin et al. 2005).With DLO it is also possible to readily compare and contrast the results obtained using discrete and smeared continuum representations of masonry constructions. For example, in the latter case, the homogenized masonry material model developed by De Buhan and De Felice (1997) can be adopted for the analysis of in-plane loaded walls, and was recently combined with DLO by Valentino et al. (2023).For a deeper understanding of how to solve DLO problems, one may refer to He et al. (2023) where a Python script is provided and explained in detail.

The current paper is organized as follows: in Section 2 the fundamental characteristics of non-periodic masonry, and a means of capturing and then classifying this type of masonry are considered; in Section 3 DLO formulations for the limit analysis of masonry structures are described, considering discrete and smeared continuum representations, as well as periodic and non-periodic masonry structures; these modelling approaches are applied to a range of examples in Section 4; and finally, in Section 5 conclusions are drawn.

2. Non-periodic masonry

2.1. Background

In general, masonry exhibits weaknesses with respect to applied actions, such as low tensile and shear strength, low ductility, and anisotropic behaviour, as outlined in Corradi et al. (2008) and Angelillo, Lourenço, and Milani (2014). Ancient masonry also has a weaker structural behaviour for many reasons (see Figure 1). An accurate analysis of the masonry is therefore needed to better understand its structural characteristics and to determine any necessary conservation.

(a) (b)

Figure 1. Failure of ancient masonry structures: (a) basilica of Saint Francis in Assisi, Italy, 1997; (b) basilica of Saint Benedict in Norcia, Italy, 2016.

The first important task when evaluating the strength of masonry buildings is to check the quality, as outlined by Borri et al. (2015). If the quality of the masonry is not sufficient then the wall will not exhibit a global response and will instead tend to disaggregate under, e.g. a seismic action. This failure mode is the most dangerous because most building collapses are immediate, and the energy required for activation is low. If the masonry quality is good enough, but there are no effective connections between walls and slabs, the building can undergo out-of-plane local mechanisms, as described by De Felice and Giannini (2001). Examples of the application of limit analysis for this type of mechanism can be found in Casapulla et al. (2021); Chiozzi et al. (2018). This kind of failure is still dangerous and requires an intermediate level of activation energy. Finally, if the connections are adequate the mechanism will be global and an in-plane failure will generally occur. This is the safest failure mode and the hardest to achieve.

With regard to masonry quality, although the resistance of stone or brick elements and the quality of mortar have an impact on the outcome (Casapulla and Argiento 2018; Krejčí et al. 2021), there are certain factors that depend solely on the texture; for example the dimensions and shape of the constituent blocks, the horizontality of mortar joints, and the staggering of vertical mortar joints. For example, in Rios et al. (2022) the influence of texture for different periodic schemes was assessed.

The failure mechanisms analysed in this work are not influenced by the strength of the blocks, as failure is always assumed to occur in the mortar joints; this is typically observed in ancient masonry structures under, e.g. seismic loads, as the mortar is usually very weak relative to the strength of the blocks. However it is noted that in certain circumstances, such as the presence of high compressive loads or strong links between walls, failure may occur within individual blocks.

2.2. Geometrical identification

A masonry bonding pattern can be defined as non-periodic when it is not possible to reproduce the whole arrangement through the repetition of smaller partitions. An example is the quasi-periodic texture introduced by Falsone and Lombardo (2007), which is often found in ancient constructions. It is composed of blocks with different sizes arranged to form horizontal courses, while the height of each course and the length of each block may vary. This kind of texture is common as it allows the direct use of stones available at hand, reducing costs, though with partial compliance with the usual rules of masonry construction. A texture that does not have horizontal courses, and that includes blocks of various shapes assorted seemingly accidentally, can be termed 'uncoursed' (Kržan et al. 2015).

One of the problems that arises for non-periodic masonry is the uniqueness of each case study. For this reason, a method of representing the texture in an analysis model is necessary. One way of proceeding is through the digital processing of images. In this case, the texture of a wall can be captured in an image that is then used to identify discrete masonry blocks and/or the geometrical parameters necessary to calibrate a homogenization approach. In Cavalagli, Cluni, and Gusella (2013) the texture was obtained from a colour photograph, while in Cluni et al. (2020) it was obtained from thermographic images. Thermographic images are helpful because they allow a masonry bonding pattern to be determined under a layer of render or other adornment, without the need for damaging intrusive work. The principle of this technique relies on the fact that part of the electromagnetic radiation emitted from a body (in the infrared range) depends on the temperature of the body itself; so when a heat flux passes through the wall, since the thermal conductivity of mortar and units is different, the temperature of the two phases will be different too, and so the location of these two elements can be identified.

Figure 2(a) shows an example of the conversion from a greyscale image to a binary filtered image, which was used by Cavalagli, Cluni, and Gusella (2013) to inform a homogenization-based analysis. In Figure 2 (b) the bonding pattern is automatically identified from the binary image via a script, for use in a rigid block analysis. The reproduction of masonry textures that reflect the characteristics of existing buildings is a topic of great interest and is currently under investigation by a number of researchers (see for example Shaqfa and Beyer (2022); Szabo, Funari, and Lourenço (2024); Wang et al. (2024)).

2.3. Classification of non-periodic masonry

Here, a classification scheme for non-periodic masonry is presented, with a particular focus on quasi-periodic textures. While a periodic texture is easy to identify, it is not straightforward to classify an irregular texture. For this reason, a simple algorithm is presented, as shown in Figure 3.

If the periodicity conditions are not fulfilled, the first step is to check the horizontality of the mortar bed joints; if this is not fulfilled, then the texture is deemed uncoursed (otherwise, the texture is quasi-periodic). The next step is to evaluate the degree of bonding between the courses. The concept of a minimum length

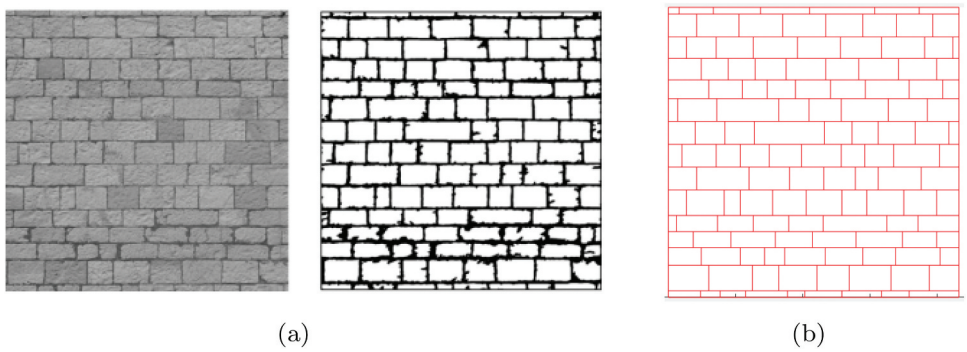

Figure 2. Automated acquisition from images: (a) greyscale image and associated binary image obtained by filtering; (b) equivalent bonding pattern obtained.

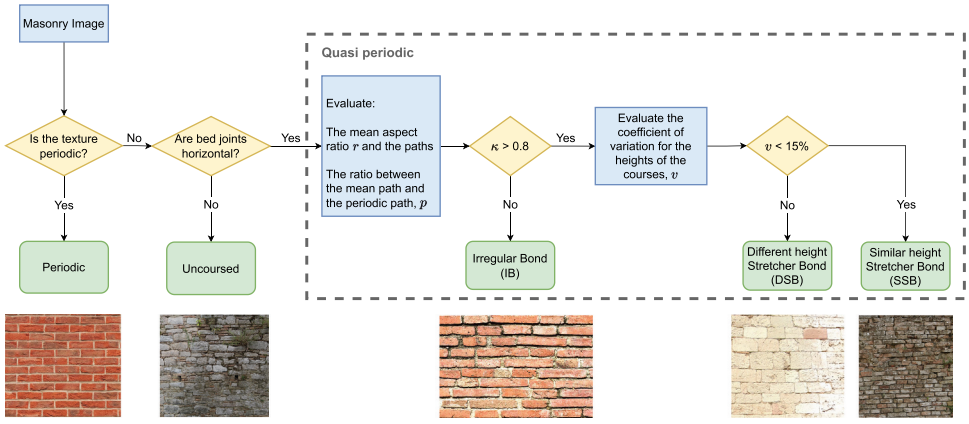

Figure 3. Non-periodic masonry classification: algorithm flowchart.

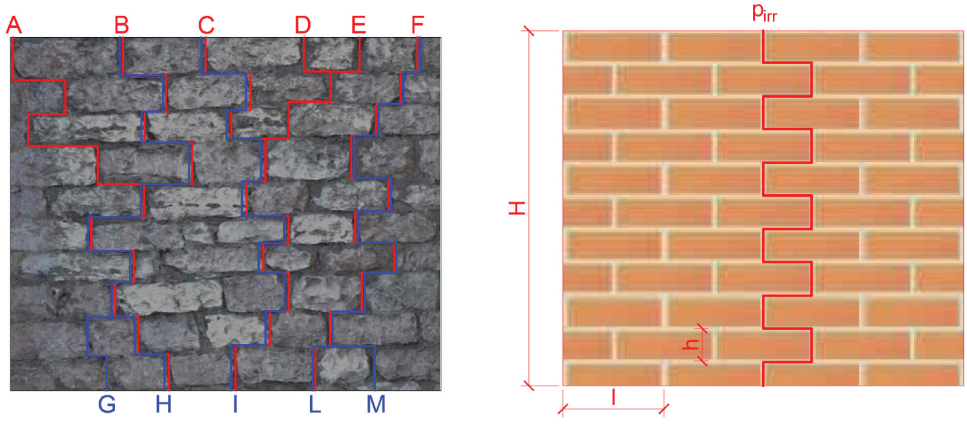

Figure 4. Evaluation of the paths through masonry: (a) shortest paths for a portion of irregular (non-periodic) masonry; (b) path for a corresponding periodic texture with the same mean *aspect ratio*.

path across the masonry panel is adopted, as used in Borri, Corradi, and De Maria (2020) and considered in Funari et al. (2022). Thus all paths of minimum length along mortar joints are drawn, from the top to the bottom (red lines) and from bottom to top (blue lines), as shown in Figure 4(a). This allows the mean value of these irregular texture (p_{irr}) path lengths to be evaluated.

The mean *aspect ratio* (r) (defined as the mean of the *aspect ratios* of all blocks) is calculated and

a corresponding periodic masonry structure with the same mean *aspect ratio* is defined. For this equivalent periodic texture, the length of the path (p_{per}) is evaluated as follows:

$$p_{per} = H + \left(\frac{H}{h} - 1\right) \cdot \frac{l}{2} \tag{1}$$

where H is the height of the irregular panel considered, h is obtained by dividing H by the number of courses of the irregular panel and $l = rh$ by definition. A visual representation of these parameters is shown in Figure 4(b).

If the block dimensions are small compared to the wall size, the formula becomes

$$p_{per} = H \cdot \left(1 + \frac{r}{2}\right) \tag{2}$$

where r is the mean aspect ratio defined previously. Though these formulae are not in the literature, they have been deduced by simple geometrical observation and by combining the concepts of *aspect ratio* and *minimum path length*.

The value of κ is then evaluated, defined as the ratio between p_{irr} and p_{per}. The value κ may be used to distinguish between an *Irregular Bond* (IB) and a *Stretcher Bond* (SB). A value lower than 0.8 is indicative of the former case, as the vertical mortar joints tend to be aligned. A value greater than 0.8 means the blocks are well staggered, indicative of the latter case.

Finally, the coefficient of variation of the heights of the courses is evaluated (κ) and used as a threshold to distinguish between a *Similar height Stretcher Bond* (SSB) and a *Different height Stretcher Bond* (DSB).

3. The discontinuity layout optimization (DLO) procedure

3.1. General DLO formulation

Discontinuity layout optimization (DLO) is a general-purpose computational limit analysis procedure that involves networks of discontinuities that interlink a base grid of nodes. Considering masonry structures, this procedure can be used to directly model masonry joints, while also modelling failure within masonry blocks if required. Stages in the DLO analysis procedure are illustrated in Figure 5. The general formulation (Gilbert, Smith, and Pritchard 2010; Smith and Gilbert 2007) can be presented in both kinematic and equilibrium forms, which are mathematical duals of each other; in this paper, the kinematic form is presented.

Thus the kinematic problem formulation for the plane strain analysis of a quasi-statically loaded, perfectly plastic cohesive-frictional body discretized using m nodal connections (slip-line discontinuities), n nodes and a single load case can be stated as follows:

$$min\ \lambda \mathbf{f}_{\mathrm{L}}^{T}\mathbf{d} = -\mathbf{f}_{\mathrm{D}}^{T}\mathbf{d} + \mathbf{g}^{T}\mathbf{p}$$

subject to

$$\mathbf{B}\mathbf{d} = \mathbf{0}$$

$$\mathbf{N}\mathbf{p} - \mathbf{d} = \mathbf{0} \tag{3}$$

$$\mathbf{f}_{\mathrm{L}}^{T}\mathbf{d} = 1$$

$$\mathbf{Q}\mathbf{p} = \mathbf{0}$$

$$\mathbf{p} \geq \mathbf{0}$$

where $\mathbf{f}_{\mathrm{D}}$ and $\mathbf{f}_{\mathrm{L}}$ are vectors containing respectively specified dead and live loads; $\mathbf{d}$ contains displacements along the discontinuities, where $\mathbf{d}^{T} = \{s_1, n_1, \omega_1, s_2, n_2, \omega_2, \ldots \omega_m\}$, and s_i, n_i and ω_i are the relative shear, normal and rotational displacements between blocks at discontinuity i (n is measured at the discontinuity midpoint); $\mathbf{g}$ represents internal energy dissipation terms for each discontinuity; $\mathbf{B}$ is a suitable $(3n \times 3m)$ compatibility matrix; $\mathbf{N}$ is a suitable flow matrix; $\mathbf{Q}$ is a suitable plastic multiplier constraint matrix; and $\mathbf{p}$ is a vector of plastic multipliers. The discontinuity displacements in $\mathbf{d}$ and the plastic multipliers in $\mathbf{p}$ are the LP variables.

The full compatibility relationship can be written as follows:

$$\mathbf{B}_i\mathbf{d}_i = \begin{bmatrix} \alpha_i & -\beta_i & 0.5\beta_i \\ \beta_i & \alpha_i & -0.5\alpha_i \\ 0 & 0 & 1/l_i \\ -\alpha_i & \beta_i & 0.5\beta_i \\ -\beta_i & -\alpha_i & -0.5\alpha_i \\ 0 & 0 & -1/l_i \end{bmatrix} \begin{bmatrix} s_i \\ n_i \\ \omega_i l_i \end{bmatrix} = \begin{bmatrix} 0 \\ 0 \\ 0 \\ 0 \\ 0 \\ 0 \end{bmatrix} \tag{4}$$

where $\alpha_i = \cos\theta_i$ and $\beta_i = \sin\theta_i$ are the direction cosines associated with the discontinuity and l_i is the length of the discontinuity.

Self-weight-effect loading is handled as follows:

$$\mathbf{f}_{\mathrm{D}}^{T}\mathbf{d} = \begin{bmatrix} W_i\beta_i & W_i\alpha_i & W\bar{p}_i/l_i \end{bmatrix} \begin{bmatrix} s_i \\ n_i \\ \omega_i l_i \end{bmatrix} \tag{5}$$

where W_i is the total weight of the strip of material lying vertically above discontinuity i, and $\bar{p}_i$ is the x-coordinate at the centroid of the strip of material relative to the centre of the chord connecting the end nodes. This approach to modelling self-weight effects allows the straightforward handling of masonry openings.

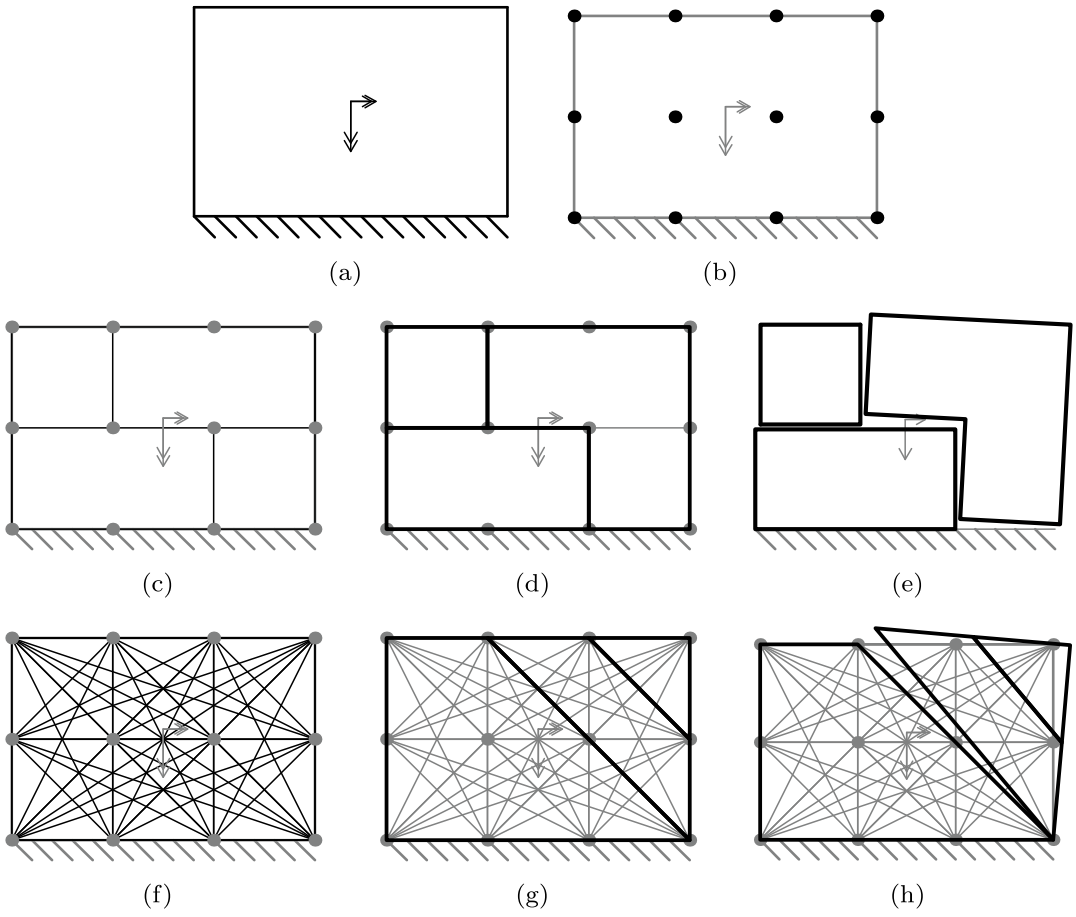

Figure 5. Stages in general DLO procedure: (a) starting problem (vertical and horizontal body forces applied to a masonry wall); (b) discretization of masonry wall using nodes; (c) interconnection of nodes along masonry joints (only); (d) identification of a critical subset of potential discontinuities using optimization (discrete block solution); (e) corresponding collapse kinematics; (f) interconnection of nodes using all potential discontinuities; (g) identification of critical subset of potential discontinuities using optimization (homogenized solution); (h) corresponding collapse kinematics.

In this paper, two models for masonry are adopted and described in the following sections. In the first model, the individual masonry units and interfaces are modelled explicitly. The second model adopts a homogenization approach, in which individual masonry units and joints are not modelled explicitly.

3.2. Existing DLO masonry models

3.2.1. Explicit representation of units in masonry constructions

When using DLO it is normal to connect each node to every other node with a potential discontinuity. Alternatively, only the potential discontinuities that coincide with joint locations can be included in the model, as shown in Figure 5(c, d, e). This provides a means of explicitly modelling the masonry units forming a wall. Modelling the associative friction and rigid body rotation on a discontinuity is enforced by adopting the following flow rule (Gilbert, Smith, and Pritchard 2010):

$$\mathbf{N}_i\mathbf{p}_i - \mathbf{d}_i = \begin{bmatrix} 1 & -1 & 0 & 0 \\ \tan\phi_i & \tan\phi_i & 0.5 & 0.5 \\ 0 & 0 & 1/l_i & -1/l_i \end{bmatrix} \begin{bmatrix} p_i^{1a} \\ p_i^{2a} \\ p_i^{1b} \\ p_i^{2b} \end{bmatrix} - \begin{bmatrix} s_i \\ n_i \\ \omega_i l_i \end{bmatrix} = 0 \tag{6}$$

The dissipation vector is given as $\mathbf{g}^T = \{c_1 l_1, c_1 l_1, c_1 l_1^2 u_1/\tan\phi_1, c_1 l_1^2 u_1/\tan\phi_1, \ldots, c_m l_m^2 u_m/\tan\phi_m\}$, where l_i and c_i are respectively the length and cohesive shear strength of discontinuity i. In this formulation the

term $\mathbf{Qp} = \mathbf{0}$ may be ignored (or alternatively, $\mathbf{Q}$ can be set to zero).

Additional discontinuities can be introduced as desired to represent, e.g. splitting or shear failure of the masonry units themselves. However, for the sake of simplicity, these are not considered in the present paper.

Note that this representation is essentially equivalent to the rigid block approach originally proposed by Livesley (1978), though here, only relative displacements along joints need to be considered as LP variables.

3.2.2. Homogenized representation of constructions comprising periodic masonry

A homogenized representation of masonry (De Buhan and De Felice 1997; Tiberti and Milani 2019) potentially allows failure to be modelled along any plane, thus following the conventional DLO approach outlined in Figure 5(f, g, h). However, the formulation involves a more extensive set of plastic multipliers that correspond with more complex matrices $\mathbf{N}$ and $\mathbf{Q}$, as described by Valentino et al. (2023).

Figure 6(a) illustrates the principle of the homogenization approach; instead of modelling individual masonry units, a representative volume element (RVE) is used to create a composite material that is applied throughout the domain. The kinematic properties of the RVE are defined by its rigid rotation Ω and strain rate tensor $\mathbf{D}$:

$$\mathbf{D} = \begin{bmatrix} D_{11} & D_{12} \\ D_{12} & D_{22} \end{bmatrix}, \tag{7}$$

where $\mathbf{D}$ is a symmetrical matrix of the strain rate tensor at any point of the domain, and D_{11}, D_{22} and D_{12} are its independent components relating to horizontal, vertical and shear strains respectively; see Figure 6 (b).

The strain rate variables D_{11}, D_{22} and D_{12} are linked to DLO displacement variables s, n, ω using

$$\begin{bmatrix} D_{11,\kappa} \\ D_{22,\kappa} \\ D_{12,\kappa} \end{bmatrix} = \begin{bmatrix} -\alpha_i\beta_i & \beta_i^2 & -\frac{\kappa\beta_i^2 l_i}{2} \\ \alpha_i\beta_i & \alpha_i^2 & -\frac{\kappa\alpha_i^2 l_i}{2} \\ \frac{\alpha_i^2}{2} - \frac{\beta_i^2}{2} & -\alpha_i\beta_i & \frac{\kappa\alpha_i\beta_i l_i}{2} \end{bmatrix} \begin{bmatrix} s_i \\ n_i \\ \omega_i \end{bmatrix} \tag{8}$$

where $\kappa = \pm 1$ is a coefficient introduced to distinguish the two end nodes of discontinuity i, and $D_{11,\kappa}$, $D_{22,\kappa}$, $D_{12,\kappa}$ are strain rate variables.

Instead of directly imposing flow rules on DLO variables, the strain rate variables D_{11}, D_{22}, D_{12} of the RVE are constrained by the flow rules governing the discontinuities within the RVE (see Figure 6):

$$D_{12}r\rho + D_{22} + \Omega r\rho \geq \mu|D_{11}r\rho + D_{12} - \Omega| \tag{9a}$$

$$D_{12}r(\rho - 1) + D_{22} + \Omega r(\rho - 1) \geq \mu|D_{11}r(\rho - 1) + D_{12} - \Omega| \tag{9b}$$

$$D_{11} \geq \mu|D_{12} + \Omega|, \tag{9c}$$

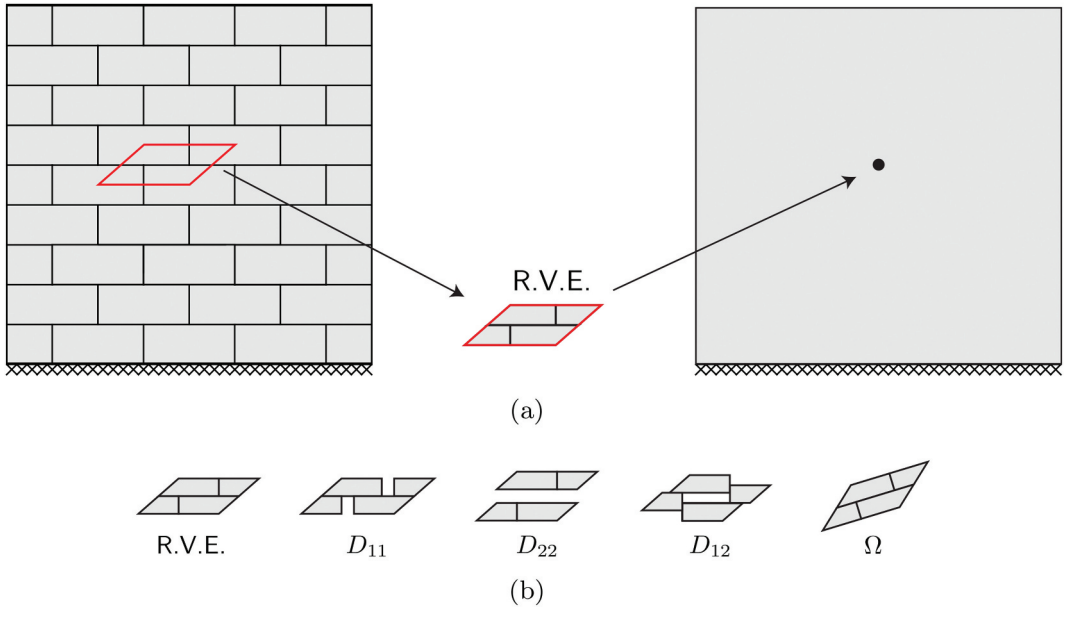

Figure 6. Homogenization approach: (a) representative volume element (RVE); (b) macroscopic strain rate variables $\{D_{11}, D_{22}, D_{12}\}$ and rigid rotation variable Ω (note that all relative displacements, rotations and flow rules are considered in the microscopic level model contained in constraint (9)).

where $\mu = \tan\phi$ is the coefficient of friction, and ρ is the interlock ratio. The associated energy dissipation within the RVE is written as follows:

$$\Pi = \frac{c\,(D_{11} + D_{22})}{\mu}, \tag{10}$$

where Π is the internal energy dissipation associated with the strain rate variables shown in Figure 6(b).

By introducing plastic multipliers $p_1, p_2, \ldots p_{12}$ that transform (6) into equality constraints, expressions (8), (9) and (10) can be rewritten to take the standard DLO form in (3); interested readers are referred to Valentino et al. (2023) for further details. It is noted that the computational cost of homogenized DLO is influenced by nodal discretization instead of wall texture or number of blocks. Therefore it provides an efficient means of analysing walls comprising a large number of blocks. A comparative analysis of CPU costs is presented in Valentino et al. (2023), evaluating the performance of homogenized DLO in contrast to rigid block methods (e.g., Cascini, Gagliardo, and Portioli 2020; Gilbert, Casapulla, and Ahmed 2006; Portioli et al. 2014).

3.3. Homogenized DLO modelling of non-periodic masonry

3.3.1. Statistical approach

Non-periodic masonry bonding patterns can potentially be modelled as equivalent periodic patterns via statistical methods. This means that walls incorporating non-periodic masonry can then be modelled via the homogenized DLO formulation described in the previous section (e.g. see Figure 7). In this case, the mean *aspect ratio r* in areas of a given wall can be evaluated and, depending on the number of distinct regions, the following cases can be defined:

- ***Uniform aspect ratio*** : an equivalent periodic masonry wall is assumed, with block *aspect ratio* calculated as the mean value of the *aspect ratio* of all blocks in a non-periodic masonry wall; see Figure 7(b).
- ***Sub-regions*** : the wall panel is instead divided into predefined *sub-regions* and for each of them, the mean value of the *aspect ratio* is evaluated; see Figure 7(c).

Note that when considering sub-regions, only blocks that are completely within a given sub-region are taken into account when evaluating the mean *aspect ratio*. Also, for the sake of simplicity, square *sub-regions* are adopted in this paper, but in general, any rectangular shape can be used provided it is representative of the texture (e.g. it contains an adequate number of blocks and courses).

3.3.2. Aspect ratio mapping method

In this approach, the homogenized DLO formulation is adapted such that the *aspect ratio r*, used in the computation of the parameters for any given discontinuity, is based on an average *aspect ratio* determined from its path across the masonry texture. For computational efficiency, the average is determined by integration across an interpolated square grid of *aspect ratio* values. First, a square grid of points is superimposed on the wall and for each grid point, the *aspect ratio* value of the block in which it resides is determined. Bilinear interpolation (Press et al. 1992) in the x and y directions is then used within each grid square to give a continuum *aspect ratio* map, as shown in Figure 7(d).

In this example, the nodal grid is very refined with respect to block size so the interpolated map accurately reflects the size and layout of the blocks. There are steep gradients across interfaces between blocks, with constant values of *aspect ratio* in between the blocks. An average *aspect ratio* $\bar{r}$ for a discontinuity is then computed by integrating the interpolated values of r along the discontinuity and dividing by the discontinuity length (L) as follows:

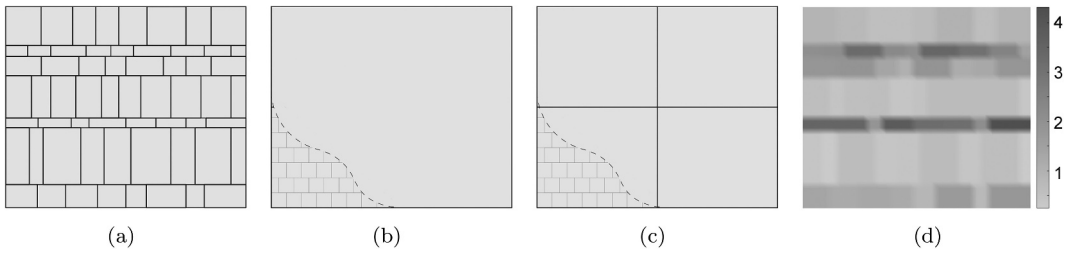

Figure 7. Methods to model a non-periodic texture with DLO: (a) discrete approach with rigid blocks and mortar interfaces; (b) homogenized model obtained considering a *uniform aspect ratio* for the entire domain; (c) homogenized model using *sub-regions* (4 in this case); (d) homogenized model obtained through mapping the *aspect ratio* in a grid of points and then interpolating the values.

$$\bar{r} = \frac{1}{L}\left(\int_0^L r\, dl\right) \tag{11}$$

The value of $\bar{r}$ is then used in Equation (9) of the homogenized DLO formulation.

4. Numerical examples

4.1. In-plane loaded square wall

4.1.1. Influence of modelling approach

To illustrate the performance of the various homogenized DLO modelling approaches, as described in Section 3.3, the in-plane behaviour of a non-periodic masonry wall was considered. For comparison, the rigid block analysis method was also employed.

Firstly, an *Irregular Bond* texture of $r = 3$, with approximately 8×24 units was generated using a purpose-written script (see Appendix for details). To model mortar joints, a Mohr-Coulomb material with cohesion $c = 0$ and coefficient of friction $\mu = 0.75$ was used, representative of historic masonry that typically has mortar with negligible cohesion. The results are shown in Table 1. It is also worth noting that the homogenized solutions are not dependent on the number of masonry units, hence, as the number of blocks increases, the results are closer to those of rigid block models.

4.1.2. Influence of masonry texture

To investigate the effect of texture on structural behaviour, square-shaped walls with different masonry textures were considered and the results are shown in Table 1. The *aspect ratio* used as input for texture generation was 3 for all cases. As in the previous example, cohesion $c = 0$ and the coefficient of friction $\mu = 0.75$. For each texture, three different block numbers were considered; 4×12, 8×24, and 16×48. For each number of blocks and each texture, five samples were generated and analysed, considering both right and left-oriented seismic actions, yielding a total of 10 adequacy factors for each scenario. The methods defined in Section 3.3.1 were then applied; the mean adequacy factor values are shown in Table 2.

Rigid block analysis models are also presented to compare to the homogenized model results. Moreover, for the 4×12 block configuration, a rigid block non-associative analysis was also undertaken, with the aim of validating the DLO rigid block and homogenized results by comparing the adequacy factors, as shown in Table 2. For this analysis, blocks at lateral boundaries with a length less than 4% of the panel length were removed to prevent the solver from picking local and non-significant mechanisms (i.e. mechanisms involving a single slender block).

Differences between the methods are later discussed to identify why some methods are better suited for certain textures than others.

Based on the rigid block associative analysis results, as shown in Table 2, the following observations can be made: as expected, the *Irregular Bond* texture has low adequacy factor values, with the mean always lower than the corresponding periodic value. Samples with relatively few masonry units exhibit higher variability than those with many units. Samples with few blocks also show higher variability compared to the periodic texture. The 4×12 *Irregular Bond* texture is the only sample where the highest adequacy factor is also lower than the periodic adequacy factor.

The rigid block non-associative analysis values are always lower than the rigid block associative analysis and higher than the homogenized solutions. This is expected and supports a hypothesis that the homogeneised analysis will be more representative of a non-

Table 1. In-plane loaded square wall — influence of modelling approach: outcomes for all methods for both seismic directions (for homogenized models, each colour shade represents a different value of aspect ratio *r*, with a lighter shade indicating a lower value of *r*.).

Dir.	Rigid block	Original *aspect ratio*	*Uniform aspect ratio*	*Sub-regions* 2 × 2	*Sub-regions* 3 × 3	*Aspect ratio* mapping method 10 × 10	*Aspect ratio* mapping method 20 × 20
left	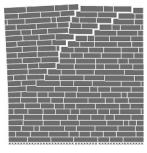	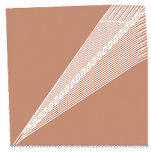	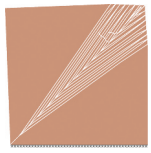	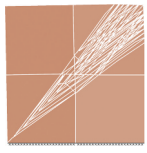	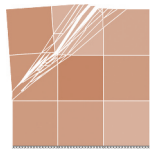		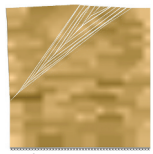
	$\lambda = 0.5592$	$\lambda = 0.4927$	$\lambda = 0.4927$	$\lambda = 0.4876$	$\lambda = 0.4786$	$\lambda = 0.4788$	$\lambda = 0.4871$
right	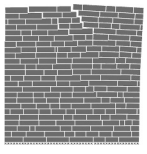		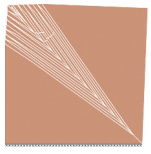	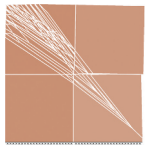	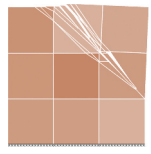	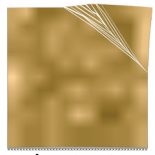	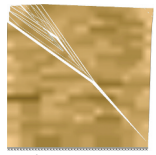
	$\lambda = 0.6105$	$\lambda = 0.4927$	$\lambda = 0.4823$	$\lambda = 0.4836$	$\lambda = 0.4729$	$\lambda = 0.4729$	$\lambda = 0.4804$

Table 2. In-plane loaded square wall — influence of masonry texture: adequacy factors λ for different modelling strategies. Square walls were generated with $r = 3$ as the starting mean value. For each number of blocks and each texture, 5 samples and both seismic action orientations were considered, amounting to 10 values. The mean values of these adequacy factors are shown, along with the coefficient of variation around the mean values for non-periodic textures.

		Rigid block		Homogenized					
						Sub-regions		*Aspect ratio* mapping method	
Texture	n° blocks	Associative	Non-associative	Original *aspect ratio*	*Uniform aspect ratio*	2×2	3×3	10×10	20×20
Periodic	4×12	0.712	0.693	0.4927	0.4755	0.4776	0.5920	0.4871	0.4908
	8×24	0.6143	–	0.4927	0.4855	0.4856	0.4758	0.4885	0.4838
	16×48	0.5455	–	0.4927	0.4892	0.4926	0.4951	0.4940	0.4942
SSB	4×12	0.6879 (4.30%)*	0.626 (10.85%)*	0.4927	0.4695	0.4697	0.4533	0.4745	0.4719
	8(10.85%)*24	0.6127 (1.51%)*	–	0.4927	0.4896	0.4915	0.4923	0.4938	0.4874
	16×48	0.5424 (1.87%)*	–	0.4927	0.4906	0.4917	0.4949	0.4928	0.4931
DSB	4×12	0.6806 (2.65%)*	0.634 (7.36%)*	0.4927	0.4696	0.4713	0.4664	0.4813	0.4839
	8×24	0.6153 (3.10%)*	–	0.4927	0.4982	0.5001	0.4989	0.4967	0.4918
	16×48	0.5472 (1.82%)*	–	0.4927	0.4933	0.4960	0.5002	0.4955	0.4873
IB	4×12	0.6372 (6.34%)*	0.523 (15.13%)*	0.4927	0.4736	0.4559	0.4191	0.4304	0.4216
	8×24	0.5884 (2.77%)*	–	0.4927	0.4806	0.4856	0.4758	0.4892	0.4926
	16×48	0.5393 (2.12%)*	–	0.4927	0.4881	0.4915	0.4894	0.4596	0.4985

*Coefficient of variation

associative rigid block analysis. The variation of rigid block non-associative analysis is also higher than in the associative friction case.

Table 2 also shows that the effect of texture is negligible when block dimensions are small compared to the size of the wall; i.e. all textures with 16×48 blocks have a very similar mean adequacy factor. An additional analysis that progressively increased the number of blocks, was conducted and the results were collected for rigid block analysis. Square walls with an *aspect ratio* $r = 3$ as a starting mean value were considered, and the number of blocks was varied from 4×12 to 20×60. For each texture, the minimum, maximum and mean values of five randomly generated samples were evaluated. Mean values are shown in Figure 8 and it is clear that the *Irregular Bond* texture generally has the lowest adequacy factor value. The convergence and decrease of adequacy factor values as the number of blocks increases (and their dimension decreases) can also be observed.

Figure 9 compares the results from different analysis methods for different masonry textures. The value of r detected by the *uniform aspect ratio* method is not exactly the same as the value chosen for the generation of texture, likely due to the presence of cut blocks at the lateral boundaries that generally have a lower r (i.e. same height and shorter length). However, this becomes negligible with a higher number of blocks, as the effect of boundary elements is less important. As shown in Figure 9, the *sub-regions* method with 4 regions (2×2) rapidly converges to the value of the *uniform aspect ratio* method when the number of blocks increases. This occurs because each region contains more blocks, making the mapping of irregularities and different *aspect ratios* less effective. With 9 regions (3×3), this effect is even more amplified; when the panel has more regions, with low block numbers, i.e. 4×12, the adequacy factor values are farther from the *uniform r* values.

These graphs use the mean value between the right-oriented and the left-oriented seismic force, as when samples are built in this way, the outcome is not highly dependent on the direction. The texture that shows the

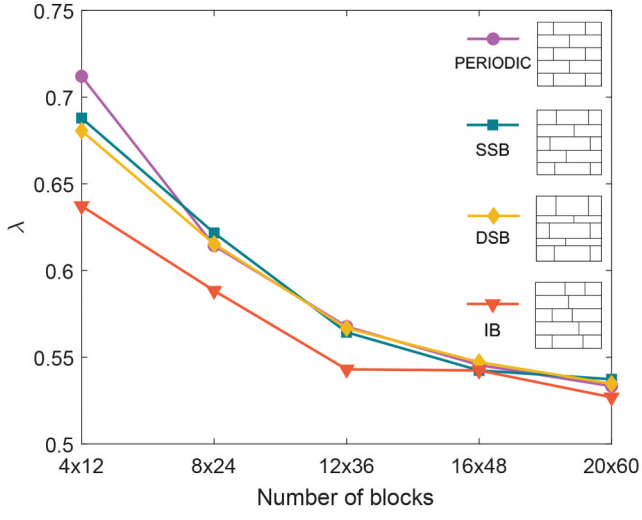

Figure 8. In-plane loaded square wall - influence of masonry texture: sensitivity of the adequacy factor to the number of units in the wall using a rigid block modelling approach (SSB = *Similar height Stretcher Bond* texture; DSB = *Different height Stretcher Bond* texture; IB = *Irregular Bond* texture).

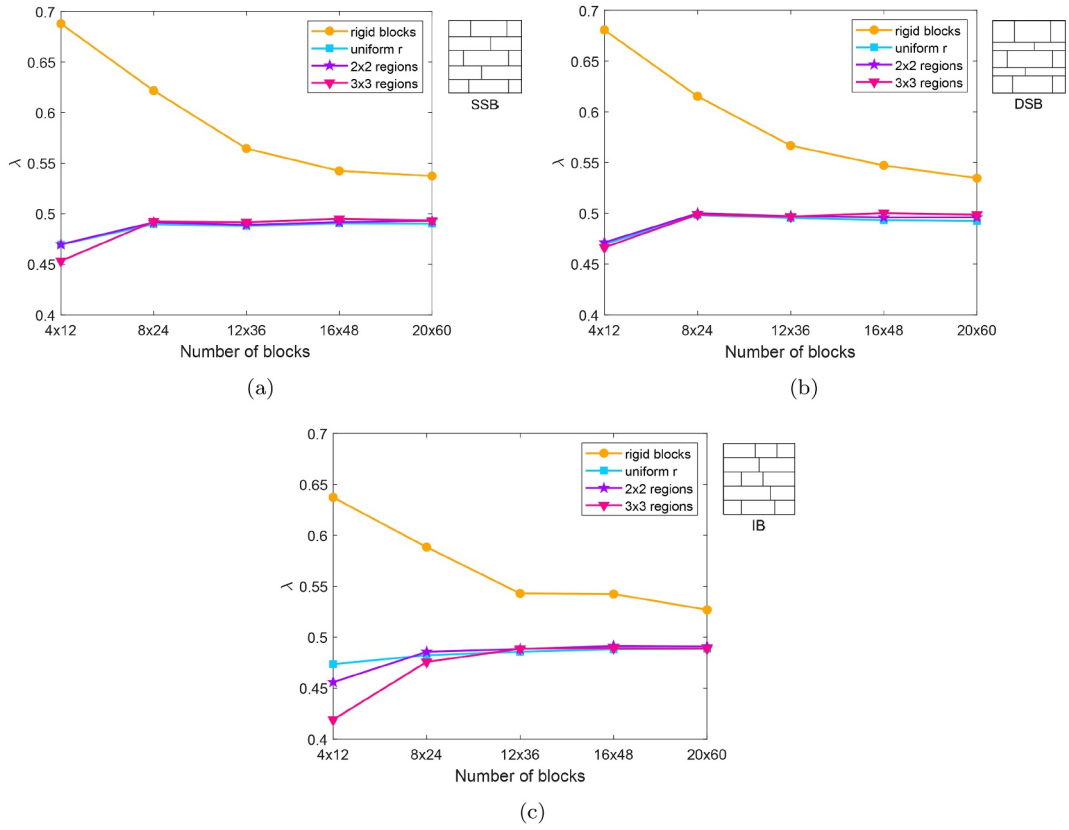

Figure 9. In-plane loaded square wall - influence of masonry texture: (a) comparison between analysis methods for an SSB texture; (b) comparison between analysis methods for a DSB texture; (c) comparison between analysis methods for an IB texture.

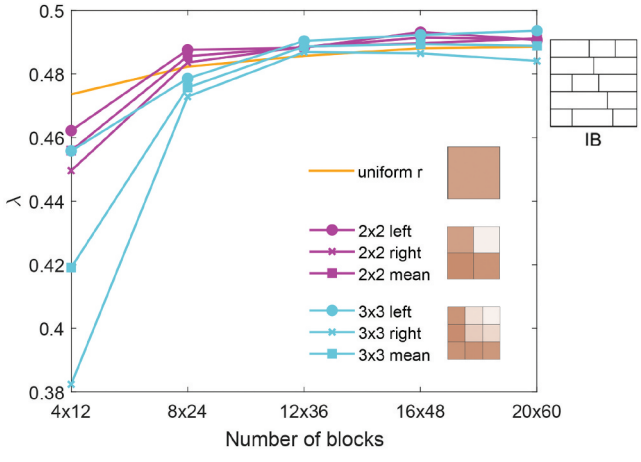

Figure 10. In-plane loaded square wall - influence of masonry texture: dependence on the direction of seismic load for the IB texture.

highest dependence on direction is IB, for which the outcome is shown in Figure 10.

4.1.3. *Influence of distribution of aspect ratio*

In the previous section, a parametric analysis was carried out. This method starts with samples randomly generated through a script that then creates blocks in the panel with a certain mean value and variation. This has two implications: first, the *aspect ratio* of the blocks is homogeneously distributed throughout the panel; second, when the number of blocks is very high, the mean *aspect ratio* will tend towards the *aspect ratio* used for the generation of the sample. However, existing masonry is often formed by blocks with specific r values, rather than smeared throughout the panel; there may be a certain spatial correlation due to the decisions and necessities of the builder. In these cases, using a *uniform* r or regions that are not representative of the problem may lead to incorrect results.

To overcome this problem, there are two possible solutions. The first is increasing the number of regions until they provide an accurate representation of the problem, and the second is using the *aspect ratio* mapping method.

A straightforward example is presented in this section to outline why, in the *aspect ratio* mapping method, it is not necessary to know the distribution of r in the panel in advance; this is because it is automatically detected by a grid and defined continuously by linear interpolation. The example panel consists of a top right quarter with the mean $r = 1$ and the rest with a mean

$r = 3$. An example textural layout, equivalent to 12×36 blocks, as used in the previous section, is shown in Figure 11(a).

From Figure 11(a), it is easy to recognize that the minimum number of *sub-regions* required to discretize the problem accurately is 2×2. However, suppose the distribution and the shape of inclusions are not so neat; in that case, a pre-analysis is likely to be necessary, where the number of regions is increased gradually until it fits the problem, as shown in Figure 11(b, c, d). However, it should be noted that if the sub-region size is reduced so much that it becomes comparable to the block size, this approach becomes less effective, as the *aspect ratio* of blocks at the regional boundary may not be accurately represented.

The results in Figure 12 show that due to the asymmetry of the problem, the mean values from each method are somewhat meaningless. For the left-oriented seismic action, the outcome for both methods is close to the *uniform r* method. This occurs because the left part of the masonry, as with the majority, has a mean value $r = 3$. In contrast, for the right-oriented seismic action, the outcome is close to the adequacy factor of the panel, if the *aspect ratio* of the entire panel matches that of the top right quarter. Although the *sub-regions* method appears to be more accurate, this is because of the simplicity of this example. The *aspect ratio* mapping method seems more unstable because it can also capture local mechanisms that require less energy to activate.

4.1.4. Influence of major heterogeneities

As outlined in Section 4.1.3, the *aspect ratio* distribution in real historical masonry constructions can sometimes be erratic. In such cases, it may often be convenient to model these explicitly, which is straightforward to achieve using DLO.

Here, two cases are considered: in the first one, there is an abrupt change in *aspect ratio* in different portions of the same wall, though interlocking remains Figure 13 (a-h); in the second one there is a vertical mortar joint between these portions instead (Figure 13 (i) - (l)).

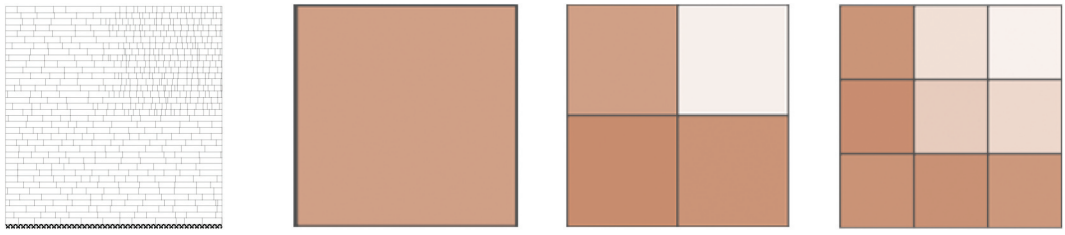

Figure 11. In-plane loaded square wall - influence of distribution of aspect ratio: (a) texture layout (12×36 blocks); (b) homogenization model for the *uniform r* method; (c) homogenization model for 2×2 *sub-regions*; (d) homogenization model for 3×3 *sub-regions* (the wall has *Irregular Bond* texture with a different *aspect ratio* in the top-right quarter (1 vs. 3).).

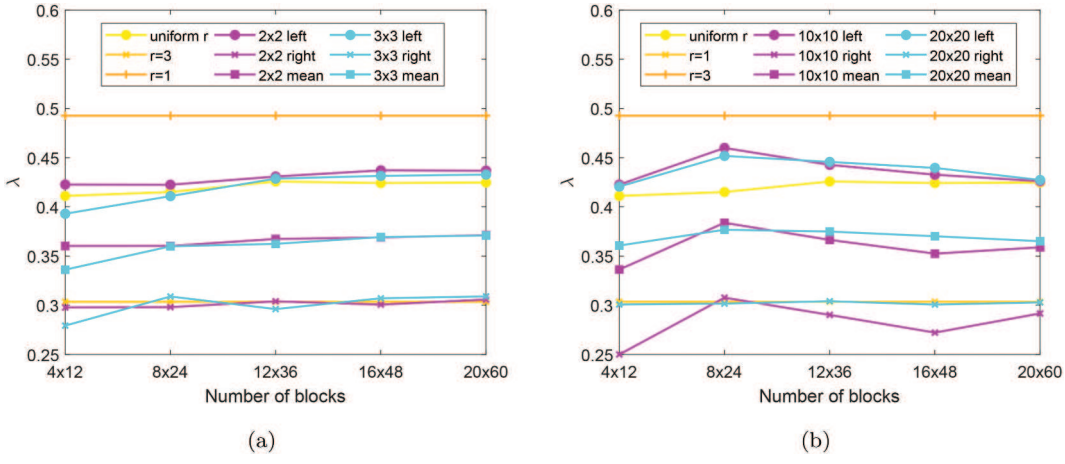

Figure 12. In-plane loaded square wall - influence of distribution of aspect ratio: (a) *sub-regions* method outcome; (b) *aspect ratio* mapping method outcome (the wall has Irregular Bond texture with a different aspect ratio in the top-right quarter (1 vs. 3); *R* = *sub-regions* method; *M* = *aspect ratio* mapping method).

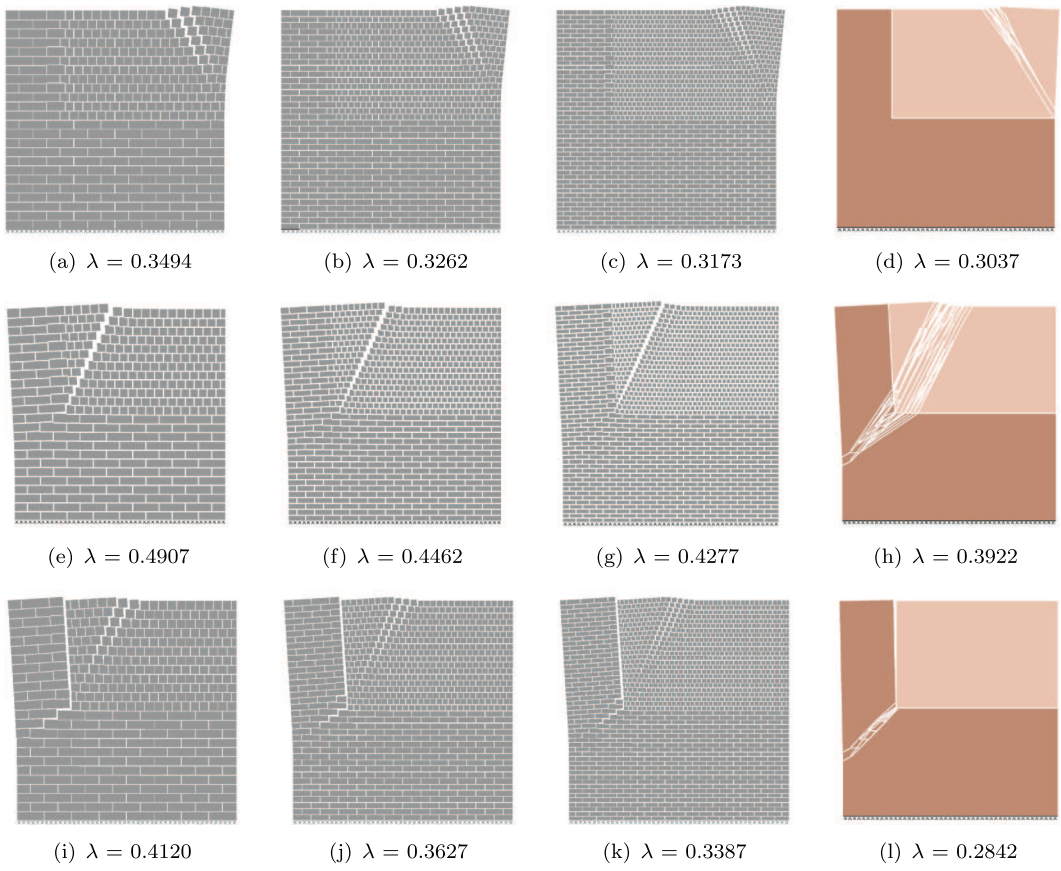

Figure 13. In-plane loaded square wall - influence of major heterogeneities: (a)-(h) heterogeneous walls with an interlocking bond between regions, (i)-(l) with a continuous joint between regions; (a, e, i) 8×24 rigid block models; (b, f, j) 12×36 rigid block models; (c, g, k) 16×48 rigid block models; (d, h, l) homogenized wall models (adjacent walls with different *aspect ratios* (3 in the bottom-left region and 1 in the upper right region), considering both right and left-oriented seismic actions).

In both cases, the *aspect ratio* was 1 in the upper-right portion and 3 in the remaining portion. The homogenized model was created by assigning different material properties to the two regions with, in the second case, a defined interface that describes the interaction properties between them (i.e. reflecting the frictional properties of a continuous mortar joint).

Solutions obtained using rigid block models, with an increasing number of masonry units, converge towards the homogenized solution. Note that for the second case, only the outcome for the left-oriented seismic action is shown; results obtained for the right-oriented seismic action outcome case match those obtained for the first case because the failure mechanisms do not involve the continuous vertical interface.

4.2. Wall with single opening

Here, a wall with a single opening, first analysed by Ferris and Tin-Loi (2001), is considered, though now also with three non-periodic texture alternatives to the periodic original, comprising full blocks with dimensions 4×1.75 units. A joint cohesion $c = 0$ and a coefficient of friction $\mu = 0.65$ were used, with the wall subject to a horizontal body force representing a seismic loading. For the original wall Figure 14(a), the outcome of which is shown in Figure 14(e), an associative friction joint model was assumed. The solution found is the same as that computed by Gilbert, Casapulla, and Ahmed (2006) for this scenario (the corresponding non-associative friction solution for this problem was $\lambda = 0.3558$). The following subsections explain how to create variations of the periodic texture reflecting the previous classification provided for quasi-periodic textures. For the sake of clarity, it should be noted that, in the case of walls with openings (this section and Sec. 4.3), variations are applied manually rather than using the algorithm described in the Appendix. This choice was made for two reasons: first, to avoid vertical joints very close to the opening; and second, to highlight the effect of vertical mortar joint alignment, particularly for the *Irregular Bond* texture under worst-case conditions.

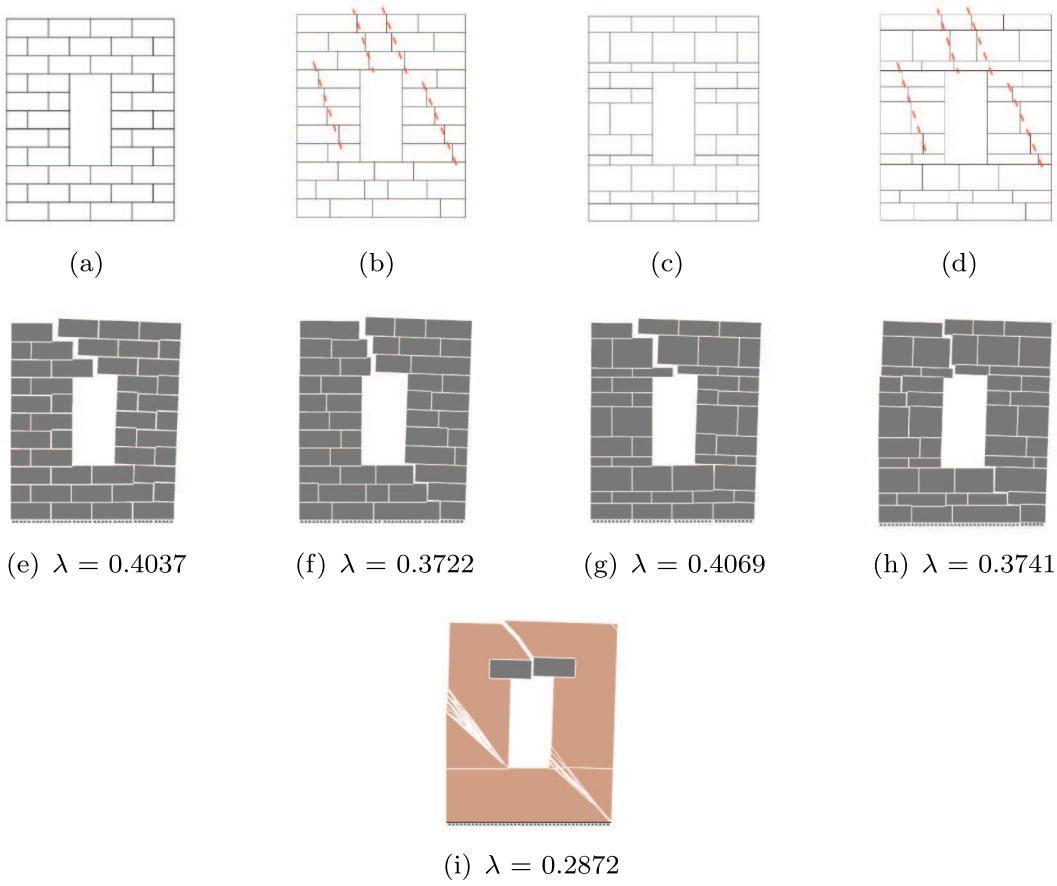

Figure 14. Wall with single opening: (a) original Ferris Tin-Loi texture; (b) alternative *Irregular Bond* texture; (c) alternative SSB/DSB texture; (d) alternative combined texture, obtained by applying both previous modifications; (e) original texture outcome; (f) *Irregular Bond* texture outcome; (g) SSB/DSB texture outcome; (h) combined texture outcome; (i) homogenized outcome.

4.2.1. Irregular Bond texture with the same mean aspect ratio

To create an *Irregular Bond* texture with the same mean *aspect ratio*, the vertical mortar joints were randomly shifted in each course, leaving the number of blocks per row unchanged; see Figure 14(b), where red dashed lines indicate an alignment of vertical mortar joints. The outcome is a reduced adequacy factor, caused by the presence of more closely aligned vertical joints.

4.2.2. SSB-DSB textures with course dependent aspect ratio

To create SSB-DSB textures with a course dependent *aspect ratio*, the position of the horizontal mortar joints were randomly shifted vertically, with the vertical mortar joint locations remaining unchanged, as shown in Figure 14(c). Thus, in this case, the *aspect ratio* of each course differs from each other. This leads to an outcome similar to that obtained for the original periodic texture, as shown in Figure 14(g).

4.2.3. A combination of previous textures

The two modifications described above were then combined; see Figure 14(d). The outcome shown in Figure 14(h) is evidently similar to the *Irregular Bond* outcome, showing that the alignment of vertical mortar joints has a major influence on the capacity of the wall. For this reason, in the classification presented in Section 2.3, a texture is identified as having an *Irregular Bond* regardless of the coefficient of variation of course height v.

Finally, for comparison, a homogenized solution is shown in Figure 14(i). This particular benchmark problem contained relatively few masonry units, and so the differences between the homogenized analysis solution and the rigid block analysis solutions are large, considering both the adequacy factor and the failure mechanism. In this case, the solution is the same for all of the quasi-periodic textures; because of the way these modified textures were generated, and by the fact the *uniform aspect ratio* method was used, the mean *aspect ratio* value was not affected. (If the *sub-regions* method or *aspect*

ratio mapping methods were used, the solution would be different for each of the modified textures considered.)

4.3. Facade with openings

The next example is a masonry facade with openings, recently considered by Valentino et al. (2023); the same adjustments to the vertical and horizontal joint locations, as described in Section 4.2, were applied. In the periodic case, each block had dimensions 0.6 × 0.3 m, resulting in an *aspect ratio* of 2. The facade had dimensions 9.0 × 10.8 m and included six openings, each measuring 1.2 × 2.1 m. Here, the coefficient of friction was taken as $\mu = 0.4$ and the cohesion as $c = 0$.

For the *Different height Stretcher Bond* (DSB) texture, the heights of two adjacent courses were modified by increasing or decreasing them by 40%; two DSB textures can be generated by switching which course is reduced in height, referred to as DSB1 and DSB2. To create an *Irregular Bond* texture (IB), vertical joints were moved to reduce block overlap to a tenth of the block length. Finally, a combined texture was generated, as explained in the previous section.

4.3.1. Seismic action

Here, the effect of a seismic action is considered. The outcome for periodic texture is shown in Figure 15(a) for the homogenized model, and Figure 15(b) for the rigid block model. Due to the symmetry of DSB textures, only the right mechanism is shown Figure 15(c, d). For IB and combination textures, both seismic orientations are shown (Figure 15 (e–h). Figure 15(e) and (f) show that IB has the weakest structural behaviour despite DSB textures having a similar adequacy factor. The combination textures inherit weak behaviour from IB; the adequacy factor is close to the IB value and lower than those of periodic and DSB values, as shown in Figure 15(g, h).

4.3.2. Rigid settlement

This section examines the effect of a rigid settlement. The outcome for the periodic texture is shown in Figure 16(a) for the homogenized model and in Figure 16(b) for the rigid block model. For the same reason as the seismic case, the DSB texture outcome is presented for just one orientation. For the DSB1 texture, there is a decrease in the adequacy factor that is not reflected in DSB2, as shown in Figure 16(c, d). This suggests that changing the row order may lead to a certain variation. Again, IB has the weakest behaviour. In this case, the failure mechanism is also orientation dependent; in Figure 16(e), cracks only occur in the outer part of the upper opening while in Figure 16(f) they also occur in the inner part. The outcome for combined textures, as in the previous application, is quite similar to the IB outcome, both in terms of the adequacy factor and failure mechanism, as shown in Figure 16 (g, h).

4.4. Commentary

Masonry constructions with a range of non-periodic bonding patterns have been investigated in this paper. Of the various analysis methods considered, the rigid block method can directly take the pattern and size of the masonry units into consideration, and provides a useful method of evaluating the behaviour of such masonry. However, as this approach requires the full geometrical characterization of the panel, it becomes cumbersome when a large number of small units are involved. Conversely, when a small number of large units are involved, the method may be prone to overestimating the true collapse load, particularly if an associative friction model is employed.

In contrast, the homogenized model does not account for the number or size of the blocks, and can only be expected to produce reliable results when the size of the constituent masonry units is small in comparison to the wall dimensions; when this is not the case the homogenized model will tend to provide lower bound solutions, albeit the degree of over-conservativism will often be high (an exception is when a failure mechanism is dominated by local effects involving, e.g. only one or two elements, such that the outcome is not representative of the overall structural behaviour of a panel).

Also, when using a homogenized model the results can be obtained rapidly if the mean *aspect ratio* of the wall is known, or when the *aspect ratio* of portions of the wall are known, depending on the method used. If a masonry panel has a small number of blocks (e.g. up to 8 x24 blocks in the examples considered), the *sub-regions* method has been observed to work well.

Masonry with a localized aspect ratio distribution can be addressed by more advanced methods such as the *aspect ratio* mapping method. However, if mapping is taken to the level of individual masonry units, then there appears to be little advantage over explicitly modelling these units using a rigid block approach.

In light of prior research, it is well established that the aspect ratio and dimensions of masonry units play a significant role in determining wall performance. Shaqfa and Beyer (2022) and Funari et al. (2022); Szabo, Funari, and Lourenço (2024) found that irregular unit sizes and poor aspect ratios reduce interlocking and

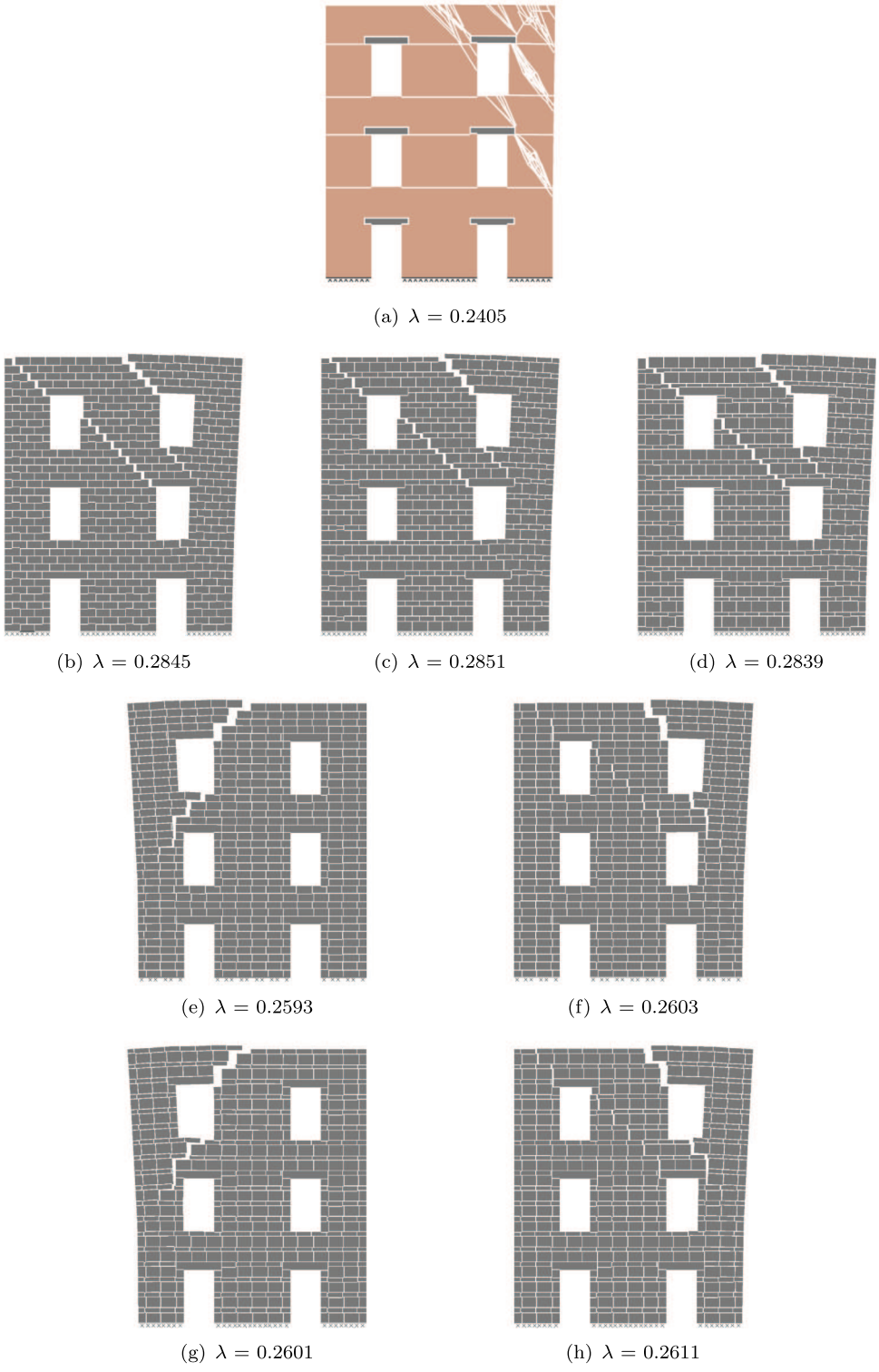

Figure 15. Facade with openings - outcomes of seismic action: (a) homogenized solution (2500 nodes); (b) periodic texture; (c) DSB1 texture; (d) DSB2 texture; (e) IB texture (left orientation); (f) IB texture (right orientation); (g) combined texture (left orientation); (h) combined texture (right orientation).

increase void sizes, leading to greater damage under stress, especially in seismic scenarios. In contrast, regular patterns with well-proportioned stones show improved load distribution and structural integrity. Similar effects were observed in this paper, with the aspect ratio emerging as a critical factor in determining wall capacity. While uniform aspect ratios across the wall improve stability, irregular patterns often contain

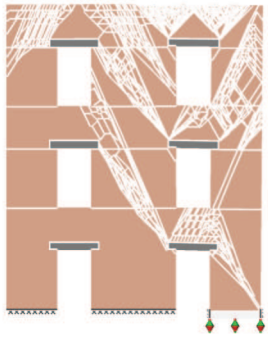

(a) $\lambda = 0.4578$

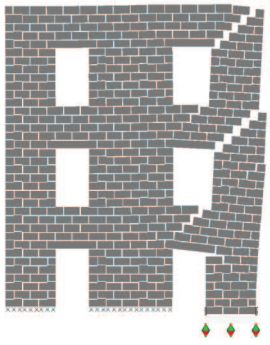

(b) $\lambda = 0.5918$

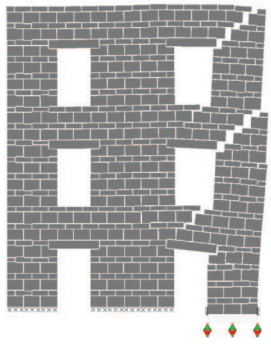

(c) $\lambda = 0.6354$

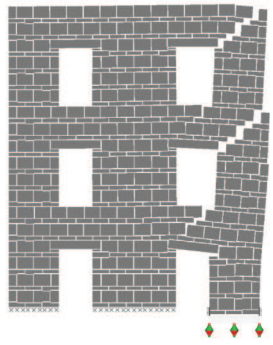

(d) $\lambda = 0.5929$

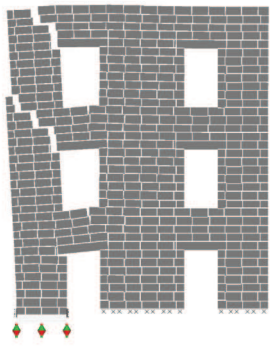

(e) $\lambda = 0.5228$

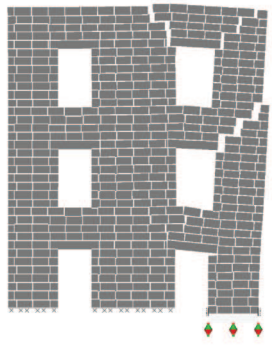

(f) $\lambda = 0.5541$

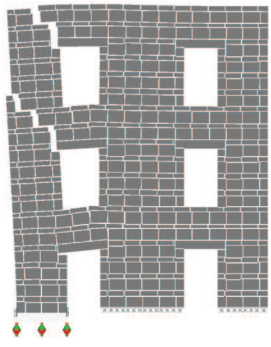

(g) $\lambda = 0.5232$

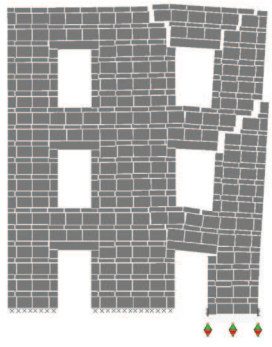

(h) $\lambda = 0.5470$

Figure 16. Facade with openings - outcomes of rigid settlement: (a) homogenized solution (2500 nodes); (b)periodic texture; (c) DSB1 texture; (d) DSB2 texture; (e) IB texture (left settlement); (f) IB texture (rightsettlement); (g) combination texture (left settlement); (h) combination texture (right settlement)

regions with blocks of high aspect ratios, which reduce load capacity and increase the likelihood of local failure.

Finally, an advantage of DLO is that homogenized and discrete modelling strategies can be mixed if there are distinct masonry patterns to be captured in certain regions. Moreover, as considered in Section 4.1.4, obvious discontinuities in the masonry can be explicitly modelled using DLO.

5. Conclusions

- A new classification procedure for non-periodic masonry textures has been proposed with three main classifications: periodic, quasi-periodic and random. The quasi-periodic classification can be further subdivided into *Similar height Stretcher Bond* (SSB), *Different height Stretcher Bond* (DSB), and *Irregular Bond* (IB). This classification is determined systematically using two parameters: the indicator κ of the degree of staggering of vertical joints and the coefficient of variation v of the height of the courses.
- The discontinuity layout optimization (DLO) method has been used to undertake 'rigid block' analyses of a range of textures and masonry panel sizes, in most cases assuming associative friction. This was achieved by restricting the locations of potential discontinuities to the locations of joints in the masonry.
- For each texture the masonry unit layout was varied randomly. The variability between the results was found to reduce with the number of units in the panel, and was greatest for walls with an *Irregular Bond* texture. For example, with a 4×12 sample, the mean adequacy factor for IB texture under seismic loading was approx. 10% lower than the periodic texture; with a 20×60 sample, this difference decreased to 1%. Overall, it is difficult to make quantitative statements; if a critical alignment of joints in an irregular masonry panel is found near the corner of a panel then low strength will result.
- In addition to rigid block analyses, the use of a homogenized modelling approach using DLO was also investigated. In this case, the masonry panel was represented by a single *aspect ratio* which can be determined from image/statistical analysis of the masonry panel or other classification techniques. For non-periodic masonry panels containing a large number of blocks (e.g. 20×60 in this case), a *uniform aspect ratio* was demonstrated to provide solutions below but within 10% of the rigid block analysis solutions.
- Homogenized DLO models effectively represent walls comprising an infinite number of masonry units. Although all of the homogenized DLO models considered herein employed an associative friction model, the computed adequacy factors were in all cases lower than corresponding rigid block models that employed a non-associative friction model, suggesting that the homogenized DLO modelling approach will generally provide safe estimates of safety.
- Three sub-variants of the homogenization approach were further considered to account for variation in the masonry within a given panel: use of a single region (*uniform aspect ratio*), subdivision of the region into sub-rectangles, and continuum mapping of the *aspect ratio* across the region, with each discontinuity adopting an average *aspect ratio* along its length. However, the trade-off between computational complexity and associated wall panel characterization does not seem to be worthwhile for each method. If the panel has been characterized it appears more straightforward to model every block explicitly.
- It is hypothesized that if major heterogeneities are individuated (e.g. two different walls joined by a continuous joint line) they can be properly modelled via the homogenization approach, which can provide a convenient 'low cost' first analysis option.

Disclosure statement

No potential conflict of interest was reported by the author(s).

Funding

Matthew Gilbert and Colin Smith acknowledge the financial support of the Engineering and Physical Sciences Research Council (EPSRC), under grant reference [EP/T001305/1].

ORCID

Mattia Schiantella http://orcid.org/0000-0002-9762-7808
Matthew Gilbert http://orcid.org/0000-0003-4633-2839
Colin C. Smith http://orcid.org/0000-0002-0611-9227
Linwei He http://orcid.org/0000-0002-2537-2244
Federico Cluni http://orcid.org/0000-0003-4204-2324

References

Angelillo, M., P. B. Lourenço, and G. Milani. 2014 Masonry behaviour and modelling. *Mechanics of Masonry Structures*, vol. (Vienna: Springer) 1–26

Anthoine, A. 1995. Derivation of the in-plane elastic characteristics of masonry through homogenization theory. *International Journal of Solids and Structures* 32 (2):137–63. doi: 10.1016/0020-7683(94)00140-R.

Binda, L., J. Pina-Henriques, A. Anzani, A. Fontana, and P. B. Lourenço. 2006. A contribution for the understanding of load-transfer mechanisms in multi-leaf masonry walls: Testing and modelling. *Engineering Structures* 28 (8):1132–48. doi: 10.1016/j.engstruct.2005.12.004.

Borri, A., M. Corradi, G. Castori, and A. De Maria. 2015. A method for the analysis and classification of historic masonry. *Bulletin of Earthquake Engineering* 13 (9):2647–65. doi: 10.1007/s10518-015-9731-4.

Borri, A., M. Corradi, and A. De Maria. 2020. The failure of masonry walls by disaggregation and the masonry quality index. *Heritage* 3 (4):1162–98. doi:10.3390/heritage3040065.

Bui, T. T., A. Limam, V. Sarhosis, and M. Hjiaj. 2017. Discrete element modelling of the in-plane and out-of-plane behaviour of dry-joint masonry wall constructions. *Engineering Structures* 136:277–94. https://www.sciencedirect.com/science/article/pii/S0141029617300913.

Casapulla, C., and L. U. Argiento. 2018. In-plane frictional resistances in dry block masonry walls and rocking-sliding failure modes revisited and experimentally validated. *Composites Part B Engineering* 132:197–213. https://www.sciencedirect.com/science/article/pii/S1359836816332590 .

Casapulla, C., L. U. Argiento, A. Maione, and E. Speranza. 2021. Upgraded formulations for the onset of local mechanisms in multi-storey masonry buildings using limit analysis. Structures 31: 380–94. doi:https://doi.org/10.1016/j.istruc.2020.11.083

Cascini, L., R. Gagliardo, and F. Portioli. 2020. LiABlock 3D: A software tool for collapse mechanism analysis of historic masonry structures. *International Journal of Architectural Heritage* 14(1) 75–94 doi:https://doi.org/10.1080/15583058.2018.1509155.

Cavalagli, N., F. Cluni, and V. Gusella. 2011. Strength domain of non-periodic masonry by homogenization in generalized plane state. *European Journal of Mechanics - A/solids* 30 (2):113–26. doi: 10.1016/j.euromechsol.2010.10.009.

Cavalagli, N., F. Cluni, and V. Gusella. 2013. Evaluation of a statistically equivalent periodic unit cell for a quasi-periodic masonry. *International Journal of Solids and Structures* 50 (25–26):4226–40. doi: 10.1016/j.ijsolstr.2013.08.027.

Chiozzi, A., G. Milani, N. Grillanda, and A. Tralli. 2018. A fast and general upper-bound limit analysis approach for out-of-plane loaded masonry walls. *Meccanica* 53 (7):1875–98. doi: 10.1007/s11012-017-0637-x.

Cluni, F., D. Costarelli, V. Gusella, and G. Vinti. 2020. Reliability increase of masonry characteristics estimation by a sampling algorithm applied to thermographic digital images. *Probabilistic Engineering Mechanics* 60:103022. doi: 10.1016/j.probengmech.2020.103022.

Cluni, F., and V. Gusella. 2004. Homogenization of non-periodic masonry structures. *International Journal of Solids and Structures* 41 (7):1911–23. doi: 10.1016/j.ijsolstr.2003.11.011.

Corradi, M., C. Tedeschi, L. Binda, and A. Borri. 2008. Experimental evaluation of shear and compression strength of masonry wall before and after reinforcement: Deep repointing. *Construction and Building Materials* 22 (4):463–72. doi: 10.1016/j.conbuildmat.2006.11.021.

Cundall, P. A., and O. D. L. Strack. 1979. A discrete numerical model for granular assemblies. *Géotechnique* 29 (1):47–65. doi: 10.1680/geot.1979.29.1.47.

D'Ayala, D., and E. Speranza. 2003. Definition of collapse mechanisms and seismic vulnerability of historic masonry buildings. *Earthquake Spectra* 19 (3):479–509. doi: 10.1193/1.1599896.

De Buhan, P., and G. De Felice. 1997. A homogenization approach to the ultimate strength of brick masonry. *Journal of the Mechanics and Physics of Solids* 45 (7):1085–104. doi: 10.1016/S0022-5096(97)00002-1.

De Felice, G., and R. Giannini. 2001. Out-of-plane seismic resistance of masonry walls. *Journal of Earthquake Engineering* 5 (2):253–71. doi: 10.1080/13632460109350394.

Falsone, G., and M. Lombardo. 2007. Stochastic representation of the mechanical properties of irregular masonry structures. *International Journal of Solids and Structures* 44 (25–26):8600–12. https://www.sciencedirect.com/science/article/pii/S0020768307002612.

Ferris, M. C., and F. Tin-Loi. 2001. Limit analysis of frictional block assemblies as a mathematical program with complementarity constraints. *International Journal of Mechanical Sciences* 43 (1):209–24. doi: 10.1016/S0020-7403(99)00111-3.

Funari, M. F., B. Pulatsu, S. Szabo´, and P. B. Lourenço. 2022. A solution for the frictional resistance in macro-block limit analysis of non-periodic masonry. *Structures* 43:847–59. https://www.sciencedirect.com/science/article/pii/S2352012422005525.

Gilbert, M., C. Casapulla, and H. M. Ahmed. 2006. Limit analysis of masonry block structures with non-associative frictional joints using linear programming. *Computers & Structures* 84 (13–14):873–87. doi: 10.1016/j.compstruc.2006.02.005.

Gilbert, M., C. C. Smith, and T. J. Pritchard. 2010. Masonry arch analysis using discontinuity layout optimisation. *Proceedings of the Institution of Civil Engineers - Engineering and Computational Mechanics* 163 (3):155–66. doi: 10.1680/eacm.2010.163.3.155.

He, L., M. Schiantella, M. Gilbert, and C. C. Smith. 2023. A python script for discontinuity layout optimization. *Structural and Multidisciplinary Optimization* 66 (7):152. doi: 10.1007/s00158-023-03583-z.

Krejčí, T., T. Koudelka, V. Bernardo, and M. Šejnoha. 2021. Effective elastic and fracture properties of regular and irregular masonry from nonlinear homogenization. *Computers & Structures* 254:106580. https://www.sciencedirect.com/science/article/pii/S0045794921001024.

Kržan, M., S. Gostič, S. Cattari, and V. Bosiljkov. 2015. Acquiring reference parameters of masonry for the structural performance analysis of historical buildings. *Bul-Letin of Earthquake Engineering* 13 (1):203–36. doi: 10.1007/s10518-014-9686-x.

Lemos, J. V. 2007. Discrete element modeling of masonry structures. *International Journal of Architectural Heritage* 1 (2):190–213. doi: 10.1080/15583050601176868.

Livesley, R. K. 1978. Limit analysis of structures formed from rigid blocks. *International Journal for Numerical Methods in Engineering* 12 (12):1853–71. doi: 10.1002/nme.1620121207.

Lyamin, A. V., S. W. Sloan, K. Krabbenhøft, and M. Hjiaj. 2005. Lower bound limit analysis with adaptive remeshing. *International Journal for Numerical Methods in Engineering* 63 (14):1961–74. doi: 10.1002/nme.1352.

Milani, G., P. B. Lourenço, and A. Tralli. 2006. Homogenised limit analysis of masonry walls, part II: Structural examples. *Computers & Structures* 84 (3–4):181–95. https://www.sciencedirect.com/science/article/pii/S0045794905003147 .

Pande, G. N., J. X. Liang, and J. Middleton. 1989. Equivalent elastic moduli for brick masonry. *Computers and Geotechnics* 8 (3):243–65. doi: 10.1016/0266-352X(89)90045-1.

Portioli, F., C. Casapulla, M. Gilbert, and L. Cascini. 2014. Limit analysis of 3D masonry block structures with non-associative frictional joints using cone programming. *Computers & Structures* 143:108–21. doi: 10.1016/j.compstruc.2014.07.010.

Press, W. H., S. A. Teukolsky, W. T. Vetterling, and B. P. Flannery. 1992. *Numerical recipes in C: The art of scientific computing*, 2nd ed. (NY), USA: Cambridge University Press.

Rios, A. J., M. Pingaro, E. Reccia, and P. Trovalusci. 2022. Statistical assessment of In-plane masonry panels using limit analysis with sliding mechanism. *Journal of Engineering Mechanics* 148 (2):04021158. doi: 10.1061/(ASCE)EM.1943-7889.0002061.

Schiantella, M., F. Cluni, and V. Gusella. 2022. Parametric analysis of failure loads of masonry textures by means of discontinuity layout optimization (DLO). *Materials* 15 (10):3691. doi: 10.3390/ma15103691.

Sejnoha, J., M. Sejnoha, J. Zeman, J. Sykora, and J. Vorel. 2008. Mesoscopic study on historic masonry. *Structural Engineering and Mechanics* 30 (1):99–117. doi: 10.12989/sem.2008.30.1.099.

Shaqfa, M., and K. Beyer. 2022. A virtual microstructure generator for 3D stone masonry walls. *European Journal of Mechanics - A/solids* 96:104656. doi: 10.1016/j.euromechsol.2022.104656.

Smith, C. C., and M. Gilbert. 2007. Application of discontinuity layout optimization to plane plasticity problems. *Proceedings of the Royal Society A: Mathematical, Physical and Engineering Sciences* 463 (2086):2461–84. doi: 10.1098/rspa.2006.1788.

Szabo, S., M. F. Funari, and P. B. Lourenço. 2024. A mason-inspired pattern generator for historic masonry structures using quality indexes. *Engineering Structures* 304:117604. doi: 10.1016/j.engstruct.2024.117604.

Tiberti, S., and G. Milani. 2019. 2D pixel homogenized limit analysis of non-periodic masonry walls. *Computers & Structures* 219:16–57. doi: 10.1016/j.compstruc.2019.04.002.

Tiberti, S., and G. Milani. 2020. 3D homogenized limit analysis of non-periodic multi-leaf masonry walls. *Computers & Structures* 234:106253. doi: 10.1016/j.compstruc.2020.106253.

Valentino, J., M. Gilbert, M. Gueguin, and C. C. Smith. 2023. Limit analysis of masonry walls using discontinuity layout optimization and homogenization. *International Journal for Numerical Methods in Engineering* 124 (2):358–81. doi: 10.1002/nme.7124.

Wang, Q., B. German Pantoja-Rosero, K. R. dos Santos, and K. Beyer. 2024. An image convolution-based method for the irregular stone packing problem in ma- sonry wall construction. *European Journal of Operational Research* 316 (2):733–53. doi: 10.1016/j.ejor.2024.01.037.

Appendix: Generation of samples

A purpose-written MATLAB script was written to generate various non-periodic wall textures, starting with the following input data:

- *aspect ratio* (r)
- number of blocks in the horizontal direction (N_x)
- mean length of the masonry units ($\bar{l}$)
- coefficient of variation for the height of the courses (v)
- coefficient of variation for the length of the units (u)
- a tolerance parameter that indicates the minimum distance between two vertical mortar joints in adjacent courses (δ)

For randomly generating the length and the height of the units, a lognormal distribution was used.

Once the *aspect ratio* (r) of the blocks and the number of blocks in the horizontal directions (N_x) are defined, a window that is ($N_x.\bar{l}$) wide and ($N_x \cdot \bar{l} \cdot r$) high can be generated. Blocks that exceed these borders were properly cut in order to obtain a rectangular shape.

For *Irregular Bond* (IB) texture, the value of v was set to 0 in order to analyse its variation with the u parameter, set to 0.3. For the *Similar height Stretcher Bond* (SSB) v was set to 0.05 and u was set to 0.2. For the *Different height Stretcher Bond* (DSB) v was set to 0.2 and u was set to 0.2. The tolerance parameter (δ) was $\bar{l}/5$ for the SSB and DSB while for the IB this was set to zero (i.e. vertical masonry joints may be aligned). This is summarized in Table A1.

Table A1. Parameters used for the generation of quasi-periodic masonry.

Parameter	SSB	DSB	IB
v	0.05	0.20	0
u	0.20	0.20	0.30
δ	$\bar{l}/5$	$\bar{l}/5$	0